Baroclinic Instability and Thermohaline Gradient Alignment in the Mixed Layer

W. R. YOUNG AND LIANGGUI CHEN

Scripps Institution of Oceanography, La Jolla, California

(Manuscript received 3 March 1994, in final form 5 June 1995)

ABSTRACT

The density of the mixed layer (ML) is approximately uniform in the vertical, but there are dynamically important horizontal gradients. The subinertial mixed layer (SML) approximation is a small Rossby number filtering of the primitive equations that isolates the low frequency ($\omega \ll f$) dynamics.

A linear stability analysis based on the SML approximation shows that the horizontal density gradients within the mixed layer (ML) support baroclinically unstable waves with inverse wavenumbers in the range 1 to 10 km. This conclusion follows from both a slab ML model, in which the horizontal velocity has no vertical shear, and a geostrophic ML model, in which the horizontal velocity is sheared according to the thermal wind relation. In the geostrophic case the instability is identical to the long wavelength limit of baroclinically unstable Eady waves.

An interesting difference between the slab and geostrophic ML is the dynamics of thermal and saline anomalies. In the slab case, thermohaline anomalies are advected without shear dispersion, and the initial T–S relation is preserved. In the geostrophic case, the shear dispersion associated with the thermal wind produces a flux of heat and salt orthogonal to the buoyancy gradient. This flux varies as the cube of the thermohaline gradients, and it acts so as to mix heat and salt while leaving buoyancy unchanged on fluid particles. The mechanism can tighten an initially diffuse T–S relation so that a cloud of points in the T–S plane condenses onto a curve.

1. Introduction

Descriptive studies of the oceanic mixed layer (ML) emphasize that structure is seen on lengths ranging from 1000 km down to the smallest horizontal scales that can be resolved with synoptic transects, say 100 m [e.g., Niiler and Reynolds 1984; Samelson and Paulson 1988; Halliwell et al. 1991]. The very long scales ($\geq$1000 km) might be characteristic of atmospheric forcing and in the ML this is the scale of climatological patterns of sea surface temperature and salinity, and the variation of Ekman transports. At scales of order 100 to 1000 km both salinity and temperature show frontal *zones*, rather than individual fronts. Resolution on still smaller scales, of order 1 to 100 km, shows convoluted patterns of salinity and temperature and fronts with widths as small as 1 km.

This hierarchy of lengths can be interpreted as the signature of geostrophic turbulence. The difficulty with developing this suggestion is that the theoretical models upon which our understanding of geostrophic turbulence is built are not entirely suitable for ML dynamics. For instance, Rhines (1976) and Salmon (1980) discuss baroclinic instability and geostrophic turbulence using the two-layer quasigeostrophic model in which the main thermocline of the ocean is idealized as the density jump between the two immiscible layers. This model can then be used to interpret ML observations if one is willing to regard ML salinity and ML temperature as being differentially and passively advected by the geostrophic turbulence in the upper of the two layers. In this case, at wavenumbers which are higher than some hypothetical cutoff of the mesoscale eddy field, one might expect a k^{-1} subrange in temperature and salinity variance (Batchelor 1959).

While not discounting this "passive advection hypothesis," it is likely that temperature and salinity in the ML are dynamically active so that baroclinic processes can generate geostrophic turbulence within the ML. The present paper is a first step in understanding the role of this shallow baroclinic instability. Using a new model of three-dimensional ML dynamics—the subinertial mixed layer (SML) approximation (Young 1994)—we study the linear stability of the simplest possible basic state: uniform meridional gradients of heat, salt, and ML depth. In this stability calculation the ML is idealized as a single active layer with internal variations in temperature and salinity. The base of the ML, which is defined by a sudden increase in density and an associated reduced gravity g', is free to deform. Thus the configuration is a $1\frac{1}{2}$-layer model but with an inhomogeneous active layer.

The SML approximation is a small Rossby number filtering approximation of the three-dimensional equations of motion. The derivation is similar to that of the

Corresponding author address: Dr. William R. Young, Scripps Institution of Oceanography, University of California at San Diego, La Jolla, CA 92093-0230.

quasigeostrophic approximation except that the single active layer has inhomogeneous temperature and salinity. Just as in quasigeostrophy, the expansion assumes that both the Rossby number and the fractional variation in layer thickness are small. In addition, the SML expansion requires that the variations in density within the layer are smaller than the density jump at the base of the layer. The horizontal pressure gradients within the layer are due to both the deformation of the base of the layer and the internal density variations of the layer. The expansion scheme assumes that these two contributions to ∇p are of the same order of magnitude. For the present paper, which is mostly concerned with linearized wave modes, the most important restriction is that the frequency is subinertial; that is, $\omega \ll f$.

The probable importance of baroclinic instability in the ML is not surprising. One expects this process to operate in a stratified and rapidly rotating fluid and many of the results outlined above can be anticipated from the classic Eady model. But the density of the ML is determined by both heat and salt, and by considering these tracers independently we identify a new process, which we call "thermohaline gradient alignment." The SML approximation shows that shear in ML velocity acts so as to align the gradients of temperature and salinity within the ML. The identification of this process, and the suggestion that it might act to produce a ML T–S relation, is probably the most important new result in this paper.

The SML approximation contains the subinertial dynamics of the familiar slab ML models (e.g., de Szoeke 1980; Schopf and Cane 1983; de Szoeke and Richman 1984; McCreary and Kundu 1988; and McCreary and Yu 1992; Ripa 1993) as a special case in which a certain nondimensional parameter (μ defined below) becomes large. But, in general, without the parametric restriction that $\mu = \infty$, the SML approximation shows that one can consistently discuss a ML in which the temperature and salinity are vertically uniform at leading order while the velocity is vertically sheared according to the thermal wind relation. A secondary goal of this paper is to compare the dynamics of a slab ML ($\mu = \infty$) with those of a geostrophic ML ($\mu = 0$). One important conclusion is that thermohaline gradient alignment relies on having some shear in the horizontal velocities and thus in the slab limit this process cannot operate.

a. The SML approximation

Our point of departure is the dimensional form of the subinertial mixed layer (SML) approximation. Three important dimensional parameters in this formulation are the undisturbed depth of the ML denoted by $\mathcal{H}$, the reduced gravity at the base of the ML denoted by g', and the Coriolis parameter denoted by f. From these parameters one can form the length $\mathcal{L} \equiv \sqrt{g'\mathcal{H}}/f$, which for the ML is about 5 to 10 km. Here $T(x, y, t)$ and $S(x, y, t)$ are the vertically averaged temperature and salinity in the mixed layer. It is convenient now to define

$$\theta \equiv \frac{\mathcal{H}}{f} g\alpha_T(T - \check{T}), \quad \sigma \equiv \frac{\mathcal{H}}{f} g\alpha_S(S - \check{S}), \quad (1.1)$$

where $\check{T}$ and $\check{S}$ are the constant temperature and salinity immediately below the base of the mixed layer. The vertically averaged ML buoyancy is then proportional to

$$\xi \equiv \theta - \sigma. \quad (1.2)$$

In this notation the density within the ML is $\rho = \check{\rho}[1 - (f/g\mathcal{H})\xi + \cdots]$, where $g \sim 10\ \mathrm{m\ s^{-2}}$ is gravity and ellipses indicate the higher-order terms in the SML expansion. These higher-order terms contain the depth dependence of the density field. The reduced-gravity g' at the base of the mixed layer is included as a large background constant in $\xi(x, y, t)$: $(\mathcal{H}/f)g' = \langle\xi\rangle$, where $\langle\ \rangle$ denotes an area average. Young (1994) denotes the vertically averaged, ML buoyancy by B. In terms of the notation introduced above $\xi = \mathcal{H}B/f$.

The introduction of the unfamiliar notation θ, σ, and ξ is justified by the ensuing simplification of the SML approximation: a clutter of f's, g''s, and $\mathcal{H}$'s is removed from the coefficients of the equations. The three fields θ, σ, and ξ all have the dimensions of streamfunction or diffusivity (L^2/T), and this simplifies order of magnitude comparisons.

The leading order horizontal velocities within the ML are

$$(u, v) = (-\psi_y, \psi_x) + (1 + \mu^2)^{-1}\left(\frac{z}{\mathcal{H}} + \frac{1}{2}\right) \times (-\xi_y - \mu\xi_x, \xi_x - \mu\xi_y), \quad (1.3)$$

where $\mu \equiv 1/f\tau_U$ and τ_U is the vertical mixing time for horizontal momentum over the depth of the mixed layer. For instance, if the vertical mixing of momentum is modeled with a viscosity ν, then $\tau_U \sim \mathcal{H}^2/\nu$. In (1.3) the streamfunction of the vertically averaged velocity in the ML is $\psi(x, y, t)$.

The velocity field in (1.3) includes a sheared ageostrophic component parallel to $\nabla\xi$. This down-pressure-gradient flow has an interesting dependence on the nondimensional parameter μ. The ageostrophic flow is proportional to $\mu(1 + \mu^2)^{-1}$, and this function has a maximum at $\mu = 1$ and vanishes if either $\mu \to 0$ or $\mu \to \infty$. If μ is small, then momentum mixing is weak and the ageostrophic velocity is small because of rotational constraints. But if μ is large so that momentum mixing is strong, then the heavy friction retards the down-pressure-gradient flow and again the ageostrophic velocity is small. The maximum ageostrophic response is achieved if $\mu = 1$. Notice that if $\mu = \infty$ in (1.3), then there is no vertical shear in the leading order ML velocity: this limit is the slab ML. The complementary

limit $\mu = 0$ is the geostrophic ML in which the shear is the "thermal wind." Between these two limits the shear is partitioned between a geostrophic component, perpendicular to $\nabla\xi$, and an ageostrophic component parallel to $\nabla\xi$. The two components have the same magnitude when $\mu = 1$.

The vertically averaged conservation laws for salt and heat in the SML approximation are

$$\sigma_t + J(\psi, \sigma) = \frac{\tau}{12}(1 + \mu^2)^{-2}\nabla\cdot[(\mathcal{J} + \mu\nabla\xi\cdot\nabla\sigma)(\mu\nabla\xi - \mathbf{z}\times\nabla\xi)],$$

$$\theta_t + J(\psi, \theta) = \frac{\tau}{12}(1 + \mu^2)^{-2}\nabla\cdot[(\mathcal{J} + \mu\nabla\xi\cdot\nabla\theta)(\mu\nabla\xi - \mathbf{z}\times\nabla\xi)], \quad (1.4a,b)$$

where τ is the vertical mixing rate for temperature and salinity and

$$\mathcal{J} \equiv J(\sigma, \theta) \quad (1.5)$$

is the Jacobian of temperature with salinity. If the vertical mixing of heat and salt is modeled with a diffusivity κ, then $\tau \sim \mathcal{H}^2/\kappa$.

The left-hand sides of (1.4) are intuitive: the vertically averaged flow advects the vertically averaged temperature and salt. The right-hand sides of (4.5) are skew, and cubically nonlinear, diffusivities due to the vertically sheared part of the velocity field in (1.3). These nonlinear terms result from consistent approximations of the fluxes $\overline{\mathbf{u}'T'}$ and $\overline{\mathbf{u}'S'}$, where the overline is a vertical average over the depth of the ML and the prime denotes the departure from the vertical average (e.g., the complete temperature in the ML is $T[x, y, z, t) = \bar{T}(x, y, t) + T'(x, y, z, t)]$.

The vorticity equation is

$$\nabla^2\psi_t - \eta_t + J(\psi, \nabla^2\psi) + \frac{1}{12}(1 + \mu^2)^{-2}[(1 - \mu^2)J(\xi, \nabla^2\xi) - 2\mu\nabla\cdot(\nabla^2\xi\nabla\xi)] = 0, \quad (1.6)$$

where the location of the base of the mixed layer is $z = -\mathcal{H} - \mathcal{H}\eta/f$ with

$$\mathcal{L}^2\eta = \psi - \frac{1}{2}\xi + \frac{\tau}{12}\mu(1 + \mu^2)^{-1}\nabla\xi\cdot\nabla\xi. \quad (1.7)$$

In (1.7), $\mathcal{L} = \sqrt{g'\mathcal{H}}/f$ is the Rossby radius of deformation. The integral constraints that $\langle\eta\rangle = 0$ and $\langle\xi\rangle = \mathcal{H}g'/f$ determine $\langle\psi\rangle$ from (1.7).

b. *The linearization of SML*

The goal of this paper is to begin the exploration of the SML approximation by studying the wave modes of a basic state in which the temperature, salinity, and streamfunction all vary linearly with the north–south coordinate y. Thus, one substitutes

$$\sigma = -\Gamma_\sigma y + \sigma'(x, y, t), \quad \theta = -\Gamma_\theta y + \theta'(x, y, t), \quad \psi = -Uy + \psi'(x, y, t) \quad (1.8)$$

into (1.4)–(1.7) and neglects all terms that are quadratic in the disturbance quantities (σ', θ', ψ'). The buoyancy is

$$\xi = -\Gamma_\xi y + \xi', \quad (1.9)$$

where

$$\Gamma_\xi \equiv \Gamma_\theta - \Gamma_\sigma, \quad \xi' \equiv \theta' - \sigma'. \quad (1.10a,b)$$

If the density of the mixed layer increases to the north, then Γ_ξ is positive. Notice that from (1.7) the depth of the base of the mixed layer is proportional to

$$\mathcal{L}^2\eta = -(C + U)y + \psi' - \frac{1}{2}\xi' - \frac{\tau}{6}\mu(1 + \mu^2)^{-1}\Gamma_\xi\xi'_y + \cdots, \quad (1.11)$$

where the ellipses represent both an inconsequential constant and the quadratic terms that arise from $\nabla\xi\cdot\nabla\xi$ in (1.7). The parameter C in (1.11) is

$$C \equiv -\frac{1}{2}\Gamma_\xi. \quad (1.12)$$

Here C is a wave speed, which will figure prominently in the remainder of this paper. The minus sign in the definition of C is included for later convenience.

We estimate an order of magnitude for the speed C by supposing that $\Delta T \sim 4$°C in $\Delta y \sim 10^6$ m and that $\alpha_T \approx 2.5 \times 10^{-4}$ (°C)$^{-1}$. We take $\mathcal{H} \sim 100$ m and $f \sim 10^{-4}$ s^{-1}. In this case, ignoring salinity, $\Gamma_\xi \sim \mathcal{H}g\alpha_T\Delta T/f\Delta y \sim 1$ cm s^{-1}. The wave speed in (1.12) is then $C \sim 1/2$ cm s^{-1}. In frontal regions Γ_ξ can easily be as large as 20 cm s^{-1} and then $C \sim 10$ cm s^{-1}.

The problem that results from linearizing the SML approximation about the basic state in (1.8) is algebraically tedious. In this paper further simplification is achieved by confining attention to two limiting cases:

(i) The slab ML, with a limit of $\mu = \infty$.
(ii) The strictly geostrophic ML, with a limit of $\mu = 0$.

Case (i) is the simpler of the two, and is disposed of first in section 2 before turning to case (ii) in section 3.

2. The wave modes of the slab ML

The limit $\mu = \infty$ corresponds to a slab ML in which the vertical mixing time for momentum is much smaller

than f^{-1}: notice that in this case the vertically sheared part of the velocities on the right-hand side of (1.3) is zero so that the leading-order velocity is simply $(u, v) = (-\psi_y, \psi_x)$. Likewise, the right-hand sides of (1.4a,b) are now zero, so that

$$\sigma_t + J(\psi, \sigma) = 0$$
$$\theta_t + J(\psi, \theta) = 0. \qquad (2.1a,b)$$

The vertical vorticity equation (1.6) collapses to

$$\mathcal{L}^2\nabla^2\psi_t - \psi_t + \frac{1}{2}\xi_t + J(\psi, \mathcal{L}^2\nabla^2\psi) = 0, \quad (2.2)$$

where $\xi = \theta - \sigma$ is the buoyancy. The displacement of the base of the mixed layer follows from simplification of (1.7):

$$\mathcal{L}^2\eta = \psi - \frac{1}{2}\xi. \qquad (2.3)$$

The term $(1/2)\xi_t$ in (2.2) couples the buoyancy and vorticity equations, and it is only because of this term that (2.2) differs from the quasigeostrophic approximation of the shallow water equations.

The system in (2.1) through (2.3) can also be derived by taking a slab mixed layer model formulated in terms of vertically integrated momentum equations (e.g., de Szoeke and Richman 1984; McCreary and Kundu 1988), and then making the well-known Rossby number expansion.

a. Nonlinear conservation laws

Standard manipulations show that the nonlinear equations in (2.1) and (2.2) have three quadratic conservation laws involving the buoyancy ξ and the streamfunction ψ. The quantities

$$\mathcal{E} \equiv \frac{1}{2}\int \mathcal{L}^2\nabla\psi\cdot\nabla\psi + \psi^2 dA$$
$$\mathcal{C} \equiv \int \xi(\mathcal{L}^2\nabla^2\psi - \psi)dA$$
$$\mathcal{Q} \equiv \frac{1}{2}\int \xi^2 dA \qquad (2.4a,b,c)$$

are all invariant provided that the fluxes vanish at the boundaries of the domain of integration.

If we consider the temperature and salinity separately, then from (2.1) there are the three obvious quadratic conservation laws for $\int \theta^2 dA$, $\int \sigma^2 dA$, and $\int \theta\sigma dA$. We also remark that with the conservative advection in (2.1) the thermohaline Jacobian $\mathcal{J} \equiv J(\sigma, \theta)$ is a material invariant:

$$\mathcal{J}_t + J(\psi, \mathcal{J}) = 0. \qquad (2.5)$$

This can be verified by direct calculation using only (2.1). But (2.5) is also obvious geometrically since

$$dA = dxdy = \mathcal{J}^{-1}d\theta d\sigma. \qquad (2.6)$$

Because the vertically averaged flow generated by ψ is incompressible in the (x, y) plane, the elemental area dA is a material invariant and from (2.1) so are $d\theta$ and $d\sigma$. Thus (2.5) follows directly from the transformation rule in (2.6).

It is true that the temperature and salinity fields, if advected by a shear flow, can "line up" in the sense that the angle χ between $\nabla\theta$ and $\nabla\sigma$ is reduced as the two fields are stretched out by differential advection. But this same stretching also increases $|\nabla\theta|$ and $|\nabla\sigma|$ so that $\mathcal{J} = |\nabla\theta||\nabla\sigma| \sin\chi$ remains equal to its initial value on material particles. It is educational to solve (2.1) with $\psi = -sy^2$ and some simple initial conditions for temperature and salinity to see how this happens in the shear flow $(u, v) = (sy, 0)$.

These remarks concerning the thermohaline Jacobian show that advection alone, as in (2.1a,b), does not produce a ML T–S relation. On one level this is obvious because if T and S are each individually conserved on fluid particles, then a cloud of points in the T–S plane remains fixed as fluid is advectively stirred. Only irreversible mixing can produce contraction of a T–S cloud and result in the formation of a T–S relation. The full significance of the thermohaline Jacobian $\mathcal{J}$ and its conservation equation (2.5) will be apparent in the next section in which we contrast the geostrophic ML ($\mu = 0$) with the present case of a slab ML ($\mu = \infty$).

b. The linearized problem and its conservation laws

Linearizing (2.1) and (2.2), and using the notation in (1.8), gives the set

$$\sigma'_t + U\sigma'_x - \psi'_x\Gamma_\sigma = 0$$
$$\theta'_t + U\theta'_x - \psi'_x\Gamma_\theta = 0$$
$$\mathcal{L}^2\nabla^2\psi'_t + U\mathcal{L}^2\nabla^2\psi'_x - \psi'_t + \frac{1}{2}(\theta'_t - \sigma'_t) = 0. \qquad (2.7a,b,c)$$

One can linearly combine (2.7a) and (2.7b) into a single equation for the perturbation buoyancy $\xi' \equiv \theta' - \sigma'$. In making this manipulation one might overlook the nontrivial solution $\sigma'(x - Ut, y) = \theta'(x - Ut, y) \neq 0$ and $\psi' = 0$. We refer to this simple solution, in which the temperature and salinity perturbations cancel in their effect on density, as the *buoyancy compensating* (BC) mode.

From the linear system in (2.7) one can prove that the following three quantities are invariant

$$\mathcal{E} \equiv \frac{1}{2}\int \mathcal{L}^2\nabla\psi'\cdot\nabla\psi' + \psi'^2 + (U/4C)\xi'^2 dA$$
$$\mathcal{Z} \equiv \frac{1}{2}\int \mathcal{L}^2(\nabla^2\psi')^2 + \nabla\psi'\cdot\nabla\psi' + (U/4C)\mathcal{L}^2\nabla\xi'\cdot\nabla\xi' dA$$

$$\mathcal{C} \equiv \int \frac{1}{4}\left(1 - \frac{U}{C}\right)\xi'^2 + \xi'(\mathcal{L}^2\nabla^2\psi' - \psi')dA. \quad (2.8a,b,c)$$

The invariants in (2.8a) and (2.8b) are positive definite if $U/C \geq 0$, so in this case there can be no linear instability. Thus, a necessary condition for instability is that

$$\frac{U}{C} < 0. \quad (2.9)$$

The explicit solution of (2.7), which now follows, shows that the necessary condition in (2.9) is also sufficient for instability.

c. Eigenmode analysis of the linear system

A systematic approach to the solution of (2.7) is the Fourier method in which one substitutes

$$\begin{pmatrix}\sigma'\\ \theta'\\ \psi'\end{pmatrix} = \exp(ikx + ily - i\omega t)\begin{pmatrix}\tilde{\sigma}\\ \tilde{\theta}\\ \tilde{\psi}\end{pmatrix} \quad (2.10)$$

into (2.7). The resulting eigenproblem is

$$\begin{pmatrix}\Omega & 0 & k\Gamma_\sigma\\ 0 & \Omega & k\Gamma_\theta\\ \frac{1}{2}\omega & -\frac{1}{2}\omega & \mathcal{L}^2p^2\Omega + \omega\end{pmatrix}\begin{pmatrix}\tilde{\sigma}\\ \tilde{\theta}\\ \tilde{\psi}\end{pmatrix} = \begin{pmatrix}0\\ 0\\ 0\end{pmatrix}, \quad (2.11)$$

where we have introduced

$$\Omega \equiv \omega - Uk$$
$$p^2 \equiv k^2 + l^2. \quad (2.12)$$

The dispersion relation is the condition that the determinant of (2.11) is zero:

$$\Omega[\Omega^2p^2\mathcal{L}^2 + \Omega\omega - Ck\omega] = 0, \quad (2.13)$$

where C is the speed defined in (1.12).

The first root of (2.13) is $\Omega = \omega - Uk = 0$ with the corresponding eigenvector

$$\begin{pmatrix}\tilde{\sigma}\\ \tilde{\theta}\\ \tilde{\psi}\end{pmatrix} = \begin{pmatrix}1\\ 1\\ 0\end{pmatrix}. \quad (2.14)$$

This is the BC mode mentioned above in the discussion after (2.7). The physical balances of the buoyancy-compensated mode are simple: the temperature and salinity perturbations cancel so that there is no buoyancy perturbation, and therefore no perturbation streamfunction. The salinity and temperature are then advected passively by the basic-state velocity U.

d. The special case $U = 0$

The other two roots of the dispersion relation (2.13) can be found by solving the quadratic equation in the square bracket. For orientation we start with the special case $U = 0$ so that $\Omega = \omega$. With this simplification there is a second root with $\omega = 0$. Since $\omega = 0$ is now a double eigenvalue, the corresponding eigenvectors span a two-dimensional space. Thus, in addition to the eigenvector in (2.14), we can conveniently pick

$$\begin{pmatrix}\tilde{\sigma}\\ \tilde{\theta}\\ \tilde{\psi}\end{pmatrix} = \begin{pmatrix}\Gamma_\sigma\\ \Gamma_\theta\\ 0\end{pmatrix} \quad (2.15)$$

as the second eigenvector corresponding to $\omega = 0$. The two eigenvectors in (2.14) and (2.15) are linearly independent provided that $\Gamma_\sigma \neq \Gamma_\theta$. In choosing (2.15) as the second eigenvector we are anticipating that $U \neq 0$ will break the degeneracy so that $\omega = 0$ is no longer a double eigenvalue. In this case one finds that the vector in (2.15) is the unique eigenvector of the mode whose frequency becomes nonzero when $U \neq 0$.

The physical interpretation of this formalism is straightforward: when $U = 0$, there are steady solutions representing arbitrary salinity *or* temperature anomalies in the ML with no vertically averaged flow ($\psi' = 0$). The eigenvector in (2.14) corresponds to the special case in which these anomalies cancel in their joint effect on density so that there is no pressure perturbation and the base of the ML is undisturbed. With the eigenvector in (2.15) the temperature and salinity perturbations are not compensated and so they produce an effect on ML density and pressure. But in this instance the base of the ML deforms so that the vertical average of the pressure gradient is zero and once again there is no vertically averaged flow ($\psi' = 0$). In this second case the mode has a depth-dependent horizontal pressure gradient that creates vertically sheared, horizontal currents in the ML. But these vertically sheared currents are very weak [$O(\mu^{-1})$] because of the rapid vertical mixing of momentum in the slab ML limit.

Still continuing with the special case $U = 0$, the third mode in (2.13) has a dispersion relation

$$\omega = \frac{Ck}{1 + \mathcal{L}^2p^2} = -\frac{\beta_{\mathrm{ML}}k}{\mathcal{L}^{-2} + k^2 + l^2}, \quad (2.16)$$

where the "ML β parameter" is $\beta_{\mathrm{ML}} \equiv -C\mathcal{L}^{-2}$. The corresponding eigenvector is

$$\begin{pmatrix}\tilde{\sigma}\\ \tilde{\theta}\\ \tilde{\psi}\end{pmatrix} = \begin{pmatrix}-(\mathcal{L}^2p^2 + 1)\Gamma_\sigma\\ -(\mathcal{L}^2p^2 + 1)\Gamma_\theta\\ C\end{pmatrix}. \quad (2.17)$$

The speed C is the zonal phase speed ω/k of long waves where long means that $(k^2 + l^2)^{-1} \gg \mathcal{L}^2$. For a ML with average depth $\mathcal{H} \sim 100$ m, stratification $g' \sim 0.01$ m s^{-2}, and $f \sim 10^{-4}$ s^{-1}, the radius of deformation is $\mathcal{L} \sim 10$ km. Thus, in this case, long waves are those whose wavelength is much greater than about 60 km. Notice that if the buoyancy is increasing to the north then Γ_ξ is positive and C is negative so that the phase speed ω/k from (2.16) is westward.

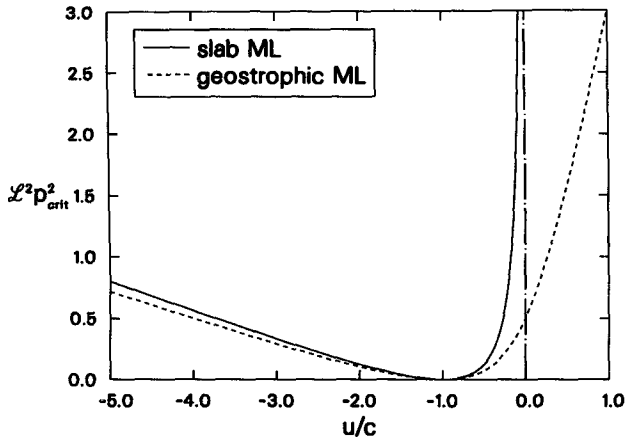

FIG. 1. The radius of the critical circle as a function of U/C: wavenumbers that lie outside the circle are unstable. In the slab case there is no instability if $U/C > 0$. In both slab and geostrophic case the critical circle contracts to the origin if $U/C = -1$, and then all wavenumbers are unstable.

At this point it is interesting to make an a posteriori assessment of the validity of the SML approximation. The SML approximation requires that the Rossby number is small, and in the present context this condition means that $\omega/f \ll 1$. To take an extreme example, consider a frontal system in which $C \sim 10$ cm s^{-1}, $l = 0$, $k^{-1} = \mathcal{L} \sim 5$ km. This choice of (k, l) maximizes the frequency in (2.16) over all wavenumbers. Then it follows that $\omega/f \sim 1/5$. Experience with the quasigeostrophic approximation suggests that $1/5$ is small enough to ensure the qualitative accuracy of the approximate dispersion relation.

e. *The general case $U \neq 0$*

We now turn to the general case when the basic-state velocity is nonzero. The structure of the BC mode in (2.14) is unchanged except that the dispersion relation is $\omega_{BC}(k, l) = Uk$ so that the compensating temperature and salinity fields are passively advected by the basic-state velocity U.

The dispersion relations of the other two modes can be found by solving the quadratic equation within the brackets in (2.13). This bracket can be rearranged as

$$(1 + \mathcal{L}^2p^2)\omega^2 - [C + U + 2U\mathcal{L}^2p^2]k\omega + \mathcal{L}^2p^2k^2U^2 = 0. \quad (2.18)$$

The two roots of the quadratic equation (2.18) are

$$\omega_F(k, l) = Uk + \frac{1}{2}\frac{k}{1 + p^2\mathcal{L}^2}[-U + C + \sqrt{(U + C)^2 + 4\mathcal{L}^2p^2UC}]$$

$$\omega_S(k, l) = Uk + \frac{1}{2}\frac{k}{1 + p^2\mathcal{L}^2}[-U + C - \sqrt{(U + C)^2 + 4\mathcal{L}^2p^2UC}], \quad (2.19a,b)$$

where the two dispersion relations have been labeled as "F" for fast or "S" for slow depending on their behavior at small wavenumbers. Specifically, if $(U + C)^2 \gg 4\mathcal{L}^2p^2UC$ and $1 \gg \mathcal{L}^2p^2$, then the dispersion relations in (2.19) can be approximated by

$$\omega_F(k, l) \approx (U + C)k$$

$$\omega_S(k, l) \approx \frac{U^2}{U + C}\mathcal{L}^2(k^2 + l^2)k. \quad (2.20a,b)$$

The fast mode has a nonzero phase speed (ω/k) at the origin of the wavenumber plane, while the slow mode is dispersive and has zero phase speed at $(k, l) = (0, 0)$.

To summarize the case when $U \neq 0$: there are three modes, BC, F, and S. The buoyancy compensated mode has the eigenvector in (2.14) and its dispersion relation is simply $\omega_{BC}(k, l) = Uk$ so that the compensated anomalies are advected by the basic-state velocity. The slow mode corresponds to the second mode, which had $\omega = 0$ when $U = 0$. The fast mode corresponds to the mode with the Rossby-like dispersion relation in (2.16). For this mode the effect of the basic-state velocity on long waves is Doppler advection as in (2.20a).

The dispersion relations in (2.19) show that there is instability when the radical is complex. This can happens if and only if $UC < 0$, and then shortwaves are unstable. Specifically, all of wavenumbers outside the circle

$$\mathcal{L}^2(k^2 + l^2) = \mathcal{L}^2p^2_{crit} \equiv -\frac{(U + C)^2}{4UC} \quad (2.21)$$

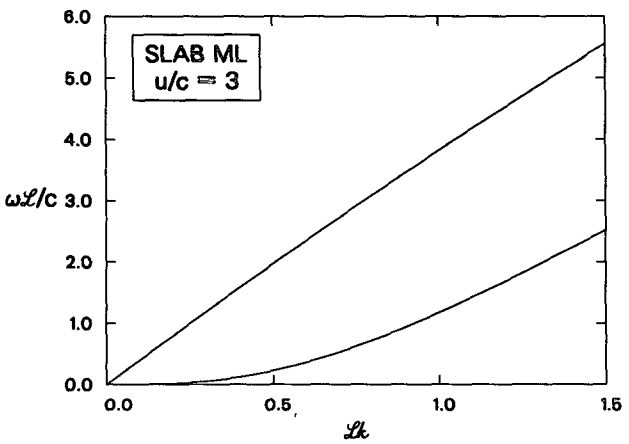

FIG. 2. Dispersion curves showing ω as function of k with $l = 0$ when $U/C = 3$ for the slab ML. In this case there is no instability. The fast mode is the branch with nonzero phase speed at $k = 0$.

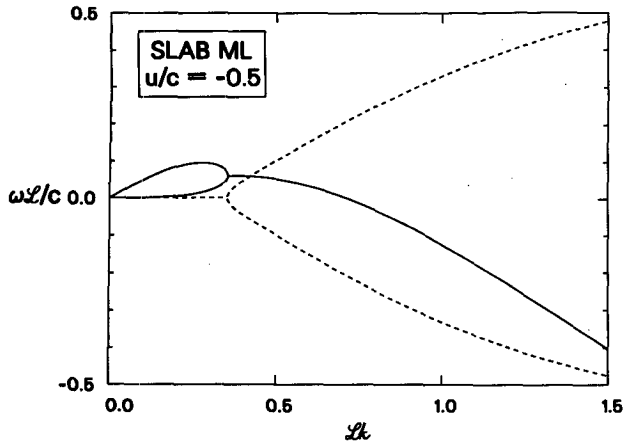

FIG. 3. Dispersion curves showing ω as function of k with $l = 0$ when $U/C = -1/2$ for the slab ML. In this, and in all subsequent figures, the real part of ω is the solid curve while the imaginary part, indicating instability, is dashed. The instability starts at $k = 1/(2\sqrt{2})$ where the two branches merge.

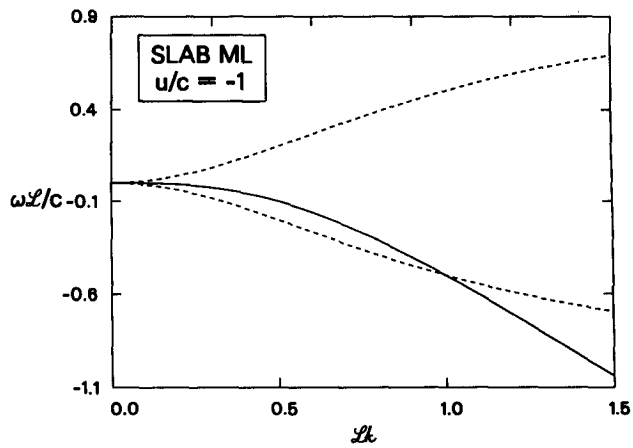

FIG. 4. Dispersion curves showing ω as function of k with $l = 0$ when $U/C = -1$ for the slab ML. In this case all wavenumbers are unstable.

in the k, l plane are unstable. The solid curve in Fig. 1 shows the radius of the critical circle in the k, l plane as a function of U/C. In Figs. 2 through 5 we plot the dispersion relation for various values of U/C and show that the onset of instability at p_{crit} results as a merger of the ω_F and ω_S branches. There is no high wavenumber cutoff for this instability. In fact, the maximum growth rate

$$\omega_i^{\max} = \frac{\sqrt{|UC|}}{\mathcal{L}} \tag{2.22}$$

is achieved by the shortest waves. (We use the notation $\omega = \omega_r + i\omega_i$.)

We remarked previously in the discussion surrounding (1.12) that for large-scale, climatological, temperature gradients of 4°C in 10^6 m the wave speed is $C \sim 1/2$ cm s^{-1}. Taking $U = -C$ and $\mathcal{L} \sim 10$ km gives an e-folding time $(\omega_i^{\max})^{-1} \sim 23$ days. This is not fast relative to many other processes in the ML. For instance, straining by the mesoscale gives a timescale that can be estimated from a 0.1 m s^{-1} velocity difference acting over 10^5 m. This gives 10^6s or about 12 days. However, notice that the maximum growth rate $\omega_i^{\max}$ in (2.22) scales with $\Gamma_\xi^{1/2}$, so that in frontal regions where $\Gamma_\xi \sim 20$ cm s^{-1} the instability could have an e-folding time of 5 days. This e-folding time is reduced even further if U is larger.

The instability has been characterized as occuring at high wavenumbers (i.e., sufficiently short waves are unstable). But this description is not accurate if $U + C = 0$. In this case (2.21) shows that the critical circle in wavenumber space contracts to the origin so that *all* wavenumbers are unstable. Thus, we can anticipate that the instability survives the addition of scale-selective damping such as diffusion of buoyancy and vorticity. The condition that $U + C$ is small is equivalent to saying that the base of the ML is nearly flat—see (1.11). This "flat base" configuration is a maximally unstable basic state in the sense that all wavenumbers are then unstable.

A recent paper by Fukamachi et al. (1993, hereafter FMP) documents a class of ML instabilities that is the same as those discussed above; there are only minor differences. In their section 3.1, FMP start with the slab ML formulated in terms of the momentum equations, rather than the SML approximation, and they do not consider the effects of temperature and salt separately, so there is no BC mode. Further, attention is confined to the case where the base of the ML is flat (i.e., $U + C = 0$), and thus FMP find that all wavenumbers are unstable. Thus, the most important difference between FMP and the present work is the remark that when $U + C \neq 0$ the ML base slopes and low wavenumbers

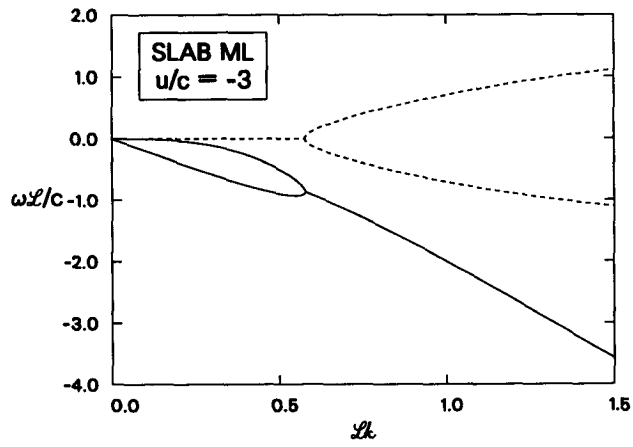

FIG. 5. Dispersion curves showing ω as function of k with $l = 0$ when $U/C = -3$ for the slab ML.

are stabilized and if $U/C > 0$ all wavenumbers are stable.

FMP also compare a numerical solution of the eigenvalue problem based on the vertically integrated momentum equations with the approximate dispersion relation in (2.18). This comparison shows good agreement between the two results over the entire range of wavenumbers displayed in Fig. 4 of FMP.

3. The wave modes of the geostrophic ML

We turn now to the limit $\mu = 0$ so that the momentum mixing is slower than an inertial period. In this case the leading order velocities in (1.3) are

$$(u, v) = (-\psi_y, \psi_x) + \left(\frac{z}{\mathcal{H}} + \frac{1}{2}\right)(-\xi_y, \xi_x). \quad (3.1)$$

In contrast to the previous section there is now vertical shear at leading order. For instance, the basic-state velocity is

$$u = U + \Gamma_\xi\left(\frac{z}{\mathcal{H}} + \frac{1}{2}\right) \quad (3.2)$$

so that the zonal component of velocity is sheared according to the thermal wind relation. In the previous section this shear was absent because the depth-dependent pressure gradient is balanced by rapid momentum mixing ($\mu = 1/f\tau_U \gg 1$) rather than the Coriolis force.

The conservation equations for heat and salt are now

$$\sigma_t + J(\psi, \sigma) = -\frac{\tau}{12}\nabla\cdot[\mathcal{J}\mathbf{z} \times \nabla\xi]$$

$$\theta_t + J(\psi, \theta) = -\frac{\tau}{12}\nabla\cdot[\mathcal{J}\mathbf{z} \times \nabla\xi], \quad (3.3a,b)$$

where $\xi = \theta - \sigma$ and $\mathcal{J} = J(\sigma, \theta)$. The vorticity equation (1.6) simplifies to

$$\mathcal{L}^2\nabla^2\psi_t - \psi_t + \frac{1}{2}\xi_t + J(\psi, \mathcal{L}^2\nabla^2\psi) + \frac{1}{12}J(\xi, \mathcal{L}^2\nabla^2\xi) = 0, \quad (3.4)$$

and the interface displacement is again given by (2.3).

Comparing equations (3.1) through (3.4) with those at the start of section 2, we see that there are two differences. The buoyancy is coupled to the vorticity by an extra term $J(\xi, \mathcal{L}^2\nabla^2\xi)$ in (3.4), and there are new and cubically nonlinear terms involving the thermohaline Jacobian $\mathcal{J} \equiv J(\sigma, \theta)$ on the right-hand side of the conservation equations (3.3). All of these new terms can be traced back to the geostrophically balanced and vertically sheared velocity proportional to $(-\xi_y, \xi_x)$ on the right-hand side of (3.1): The $J(\xi, \nabla^2\xi)$ is Reynolds stress forcing of the vertical vorticity produced by this geostrophic velocity and the $\nabla\cdot[\mathcal{J}\mathbf{z} \times \nabla\xi]$ term is the shear dispersion of temperature and salt that results from the same sheared geostrophic velocity (Young 1994).

a. Nonlinear conservation laws

The quantities $\mathcal{C}$ and $\mathcal{Q}$ defined in (2.4b) and (2.4c) are also invariants of the system in (3.1) through (3.4). The energy-like invariant, $\mathcal{E}$ in (2.4a), must be modified to

$$\mathcal{E} \equiv \frac{1}{2}\int \mathcal{L}^2\nabla\psi\cdot\nabla\psi + \psi^2 - \frac{1}{12}\mathcal{L}^2\nabla\xi\cdot\nabla\xi dA. \quad (3.5)$$

Notice that $\mathcal{E}$ is no longer positive definite if $U/C > 0$. This is the first indication that the stability properties of the geostrophic ML differ qualitatively from those of the slab ML.

Now that the right-hand sides of (3.3) are no longer zero the quadratic thermal and haline fields are no longer invariant. Simple manipulations show that

$$\frac{d}{dt}\frac{1}{2}\int \theta^2 dA = -\frac{\tau}{12}\int \mathcal{J}^2 dA$$

$$\frac{d}{dt}\frac{1}{2}\int \sigma^2 dA = -\frac{\tau}{12}\int \mathcal{J}^2 dA$$

$$\frac{d}{dt}\int \sigma\theta dA = -\frac{\tau}{6}\int \mathcal{J}^2 dA. \quad (3.6a,b,c)$$

Because the rhs of (3.6a,b) is negative definite, we can anticipate that the new terms on the rhs of (3.3) produce downgradient mixing of temperature and salinity.

Remarkably, the nonlinear downgradient mixing of T and S in (3.3) does not change the buoyancy. In fact, the right-hand sides of (3.3a) and (3.3b) cancel if one forms a single equation for $\xi \equiv \theta - \sigma$. Thus, the buoyancy of any fluid particle is constant while this irreversible mixing of heat and salt proceeds. Since the mean square temperature θ^2 and mean square salinity σ^2 both decrease, while the mean square buoyancy $\xi^2 = \theta^2 + \sigma^2 - 2\sigma\theta$ remains constant, the mixing process must create a negative cross-correlation between the temperature and salinity.

b. Thermohaline gradient alignment

The remarks in the previous section concerned mainly the dynamics of thermohaline variance. In this section we supplement these arguments, and reinforce our previous conclusions, with some deductions concerning thermohaline gradients.

In the slab limit described in section 2 we found that the Jacobian $\mathcal{J} \equiv J(\sigma, \theta)$ was conserved on material particles—see (2.5). Here $\mathcal{J}$ reappears on the right-hand side of (3.6) as the quantity that drives the global decrease of the squared temperature and salinity fields. One can now show by direct manipulations of (3.3) that

$$\mathcal{J}_t + J(\psi, \mathcal{J})$$

$$= \frac{\tau}{12} \nabla\cdot[\nabla\cdot(\mathcal{J}\mathbf{z} \times \nabla\xi)(\mathbf{z} \times \nabla\xi)]. \quad (3.7)$$

The formidable right-hand side of (3.7) produces a very simple result when one forms the integral balance for the squared Jacobian:

$$\frac{d}{dt}\int \mathcal{J}^2 dA = -\frac{\tau}{6}\int [\nabla\cdot(\mathcal{J}\mathbf{z} \times \nabla\xi)]^2 dA. \quad (3.8)$$

Thus the globally integrated, squared Jacobian of temperature and salinity also decreases monotonically as a result of the mixing terms on the right-hand side of (3.3a,b). Notice that in the slab case $\int \mathcal{J}^2 dA$ is constant because the right-hand side of (2.5) is zero.

The integrals above show that there is a process of "thermohaline gradient alignment" that is driven by the right-hand sides of (3.3). As a thought experiment, suppose that arbitrary distributions of θ and σ are established initially and then evolve freely according to geostrophic SML dynamics. We can demonstrate that (i) $\int \mathcal{J}^2 dA \to 0$ as $t \to \infty$ and (ii) $\mathcal{J} = |\nabla\theta||\nabla\sigma| \sin\chi \to 0$ because $\sin\chi \to 0$, rather than by simply mixing the temperature and salinity gradients $|\nabla\theta|$ and $|\nabla\sigma|$ to zero.

To prove the first point: because $\int \theta^2 dA \geq 0$, eventually the right-hand sides of (3.6a) must become zero. [Notice that (3.8) alone merely enables one to conclude that $\int \mathcal{J}^2 dA$ decreases monotonically: it does not allow one to reach the stronger result that $\int \mathcal{J}^2 dA \to 0$.] To prove the second point: because that $\int (\theta - \sigma)^2 dA$ is constant the mixing process cannot result in the uniform state $\theta = \sigma = 0$: some thermohaline gradients have to survive as $t \to \infty$. Thus, one concludes that the thermohaline Jacobian becomes zero because the temperature and salinity gradients become parallel ($\chi = 0$) or "antiparallel" ($\chi = \pi$).

Thermohaline gradient alignment must compete with the various processes that force the ML and create nonparallel temperature and salinity distributions. We also emphasize that the deductions above depend on having a geostrophic mixed layer ($\mu = 0$). This assumption greatly simplifies the mixing terms on the rhs of the thermohaline conservation laws in (1.4). (But not as greatly as the case $\mu = \infty$, which choice makes the rhs zero.)

Despite these caveats one can now begin to argue that there is an identifiable dynamical process that might be responsible for forming a ML T–S relation. The following linear stability analysis, though limited to small disturbances, provides a more concrete illustration of how thermohaline gradient alignment works.

c. *The linearized problem and its conservation laws*

We now turn to the linearized dynamics using the decomposition in (1.8). Notice that the thermohaline Jacobian of the basic state is zero and that to linear order the perturbation Jacobian is

$$\mathcal{J} = -\Gamma_\theta \sigma'_x + \Gamma_\sigma \theta'_x. \quad (3.9)$$

Linearizing (3.3) and (3.4) gives the set

$$\sigma'_t + U\sigma'_x - \psi'_x\Gamma_\sigma = \frac{\tau}{12}\Gamma_\xi(\Gamma_\theta\sigma'_{xx} - \Gamma_\sigma\theta'_{xx})$$

$$\theta'_t + U\theta'_x - \psi'_x\Gamma_\theta = \frac{\tau}{12}\Gamma_\xi(\Gamma_\theta\sigma'_{xx} - \Gamma_\sigma\theta'_{xx})$$

$$\mathcal{L}^2\nabla^2\psi'_t + U\mathcal{L}^2\nabla^2\psi'_x - \psi'_t + \frac{1}{2}\xi'_t$$

$$+ \frac{1}{12}\Gamma_\xi\mathcal{L}^2\nabla^2\xi'_x = 0, \quad (3.10a,b,c)$$

where $\xi' = \theta' - \sigma'$. The quantity $\mathcal{C}$ defined in (2.8c) is an invariant of the system above. The other two invariants (2.8a) and (2.8b) are now

$$\mathcal{E} \equiv \frac{1}{2}\int \mathcal{L}^2\nabla\psi'\cdot\nabla\psi' + \psi'^2 + (U/4C)\xi'^2$$

$$- \frac{1}{12}\mathcal{L}^2\nabla\xi'\cdot\nabla\xi' dA.$$

$$\mathcal{Z} \equiv \frac{1}{2}\int \mathcal{L}^2(\nabla^2\psi')^2 + \nabla\psi'\cdot\nabla\psi'$$

$$+ (U/4C)\nabla\xi'\cdot\nabla\xi' - \frac{1}{12}\mathcal{L}^2(\nabla^2\xi')^2 dA. \quad (3.11)$$

Because $\mathcal{E}$ and $\mathcal{Z}$ are no longer of definite sign when $U/C > 0$, there is no sufficient condition for stability. The detailed calculation below shows that the basic state in (1.8) is unstable for all values of U/C.

From (3.10a) and (3.10b) one can easily show that the linearized thermohaline Jacobian in (3.9) evolves according to

$$\mathcal{J}_t + U\mathcal{J}_x = D_\parallel \mathcal{J}_{xx}, \quad (3.12)$$

where

$$D_\parallel = \frac{\tau}{12}\Gamma_\xi^2 = \frac{\tau}{3}C^2 \quad (3.13)$$

is a shear diffusivity acting parallel to the contours of the basic-state buoyancy field $-\Gamma_\xi y$ so that $D_\parallel$ is an "epipycnal" diffusivity. It follows from (3.12) that

$$\frac{d}{dt}\int \mathcal{J}^2 dA = -2D_\parallel \int \mathcal{J}_x^2 dA. \quad (3.14)$$

This equation is the linear analog of the nonlinear result (3.8).

d. *Eigenmode analysis of the linear system*

The Fourier method used in section 2, when applied to the system in (3.10), yields the dispersion relation

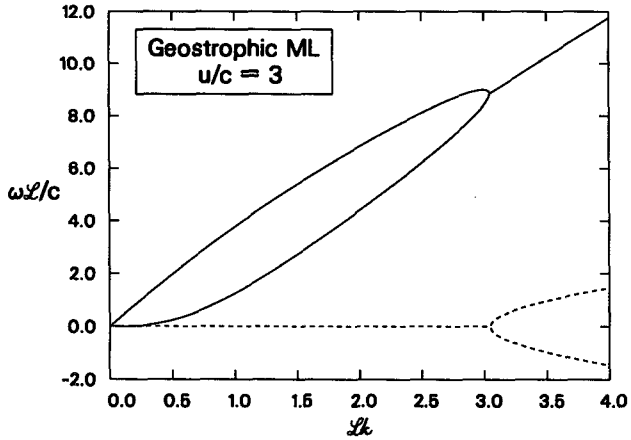

FIG. 6. Dispersion curves showing ω as function of k with $l = 0$ when $U/C = 3$ for the geostrophic ML. In this particular figure the range of the k axis has been expanded to show the merger of the two branches and the onset of high wavenumber instability.

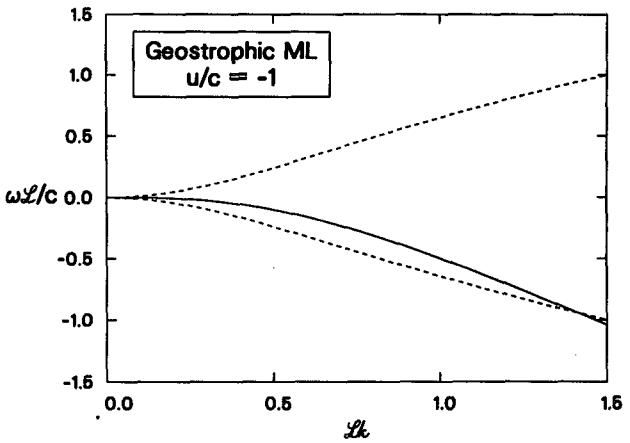

FIG. 8. Dispersion curves showing ω as function of k with $l = 0$ when $U/C = -1$ for the geostrophic ML. In this figure, as in Fig. 4, all wavenumbers are unstable.

$$(\Omega + iD_{\|}k^2)\left[\Omega^2 p^2 \mathcal{L}^2 + \omega\Omega - Ck\omega + \frac{1}{3}C^2 p^2 \mathcal{L}^2 k^2\right] = 0, \quad (3.15)$$

where $p \equiv k^2 + l^2$ and $\Omega \equiv \omega - Uk$. The corresponding result in the slab ML limit is (2.13). The first root of (3.15) is when the term within parentheses vanishes. This gives

$$\omega_{BC}(k, l) \equiv Uk - iD_{\|}k^2. \quad (3.16)$$

This is the buoyancy compensated mode with the eigenvector in (2.14). The compensated anomalies are advected by the basic-state velocity U. But in this case the anomalies are also shear dispersed along the direction of the basic-state buoyancy field. Notice that the diffusion coefficient $D_{\|}$ in (3.13) depends quadratically on the basic-state buoyancy gradient. As a nominal numerical estimate, suppose that the vertical mixing time τ is 10^5 s and that the $C \sim 1/2$ cm s^{-1}, corresponding to a large-scale climatological buoyancy gradient [see the earlier discussion after (1.12)]. In this case $D_{\|} \sim 1$ m^2 s^{-1}. However, in frontal zones C is of order 0.1 m s^{-1}, and in this case $D_{\|} \sim 300$ m^2 s^{-1}.

Notice that $D_{\|}$ in (3.13) increases as τ becomes larger: weaker vertical mixing (big τ) means stronger horizontal mixing (big $D_{\|}$). This is analogous to the well-known inverse dependence of the shear diffusion coefficient on molecular diffusivity (Taylor 1953).

The other two roots of (3.15) are determined by the bracket vanishing. This condition is equivalent to

$$(1 + \mathcal{L}^2 p^2)\omega^2 - [C + U + 2U\mathcal{L}^2 p^2]k\omega + \mathcal{L}^2 p^2\left[U^2 + \frac{1}{3}C^2\right]k^2 = 0. \quad (3.17)$$

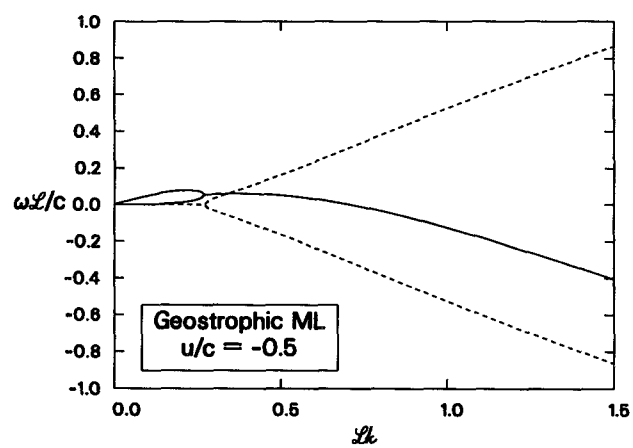

FIG. 7. Dispersion curves showing ω as function of k with $l = 0$ when $U/C = -0.5$ for the geostrophic ML. In this figure the ultraviolet divergence of the growth rate is evident.

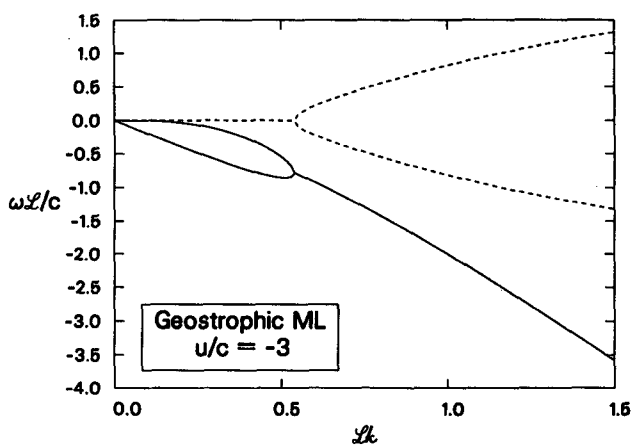

FIG. 9. Dispersion curves showing ω as function of k with $l = 0$ when $U/C = -0.3$ for the geostrophic ML.

In broad terms the two solutions of (3.17) are similar to those discussed in section 2—compare Figs. 6–9 with Figs. 2–5. At small wavenumbers (meaning that both $C + U \gg 2U\mathcal{L}^2p^2$ and $1 \gg \mathcal{L}^2p^2$) the two roots of (3.17) are

$$\omega_F(k, l) \approx (U + C)k$$

$$\omega_S(k, l) \approx \frac{U^2 + (C^2/3)}{U + C}\mathcal{L}^2(k^2 + l^2)k, \quad (3.18a,b)$$

and these results are very similar to the approximations in (2.20).

The exact solution of the quadratic in (3.17) is

$$\omega_F(k, l) = \frac{1}{2}\frac{k}{1 + \mathcal{L}^2p^2}[C + U + 2U\mathcal{L}^2p^2 + \sqrt{\Delta}]$$

$$\omega_S(k, l) = \frac{1}{2}\frac{k}{1 + \mathcal{L}^2p^2}[C + U + 2U\mathcal{L}^2p^2 - \sqrt{\Delta}], \quad (3.19a,b)$$

where $\Delta(p^2)$ is the discriminant

$$\Delta(p^2) \equiv \left[1 - \frac{4}{3}\mathcal{L}^2p^2(1 + \mathcal{L}^2p^2)\right]C^2 + 2(1 + 2\mathcal{L}^2p^2)CU + U^2. \quad (3.20)$$

Instability occurs when Δ changes sign, and this condition defines a critical circle $k^2 + l^2 = p_{crit}^2$ in the (k, l) plane. Wavenumbers outside the circle are unstable and those inside are stable. The radius of the critical circle is given by

$$\mathcal{L}^2p_{crit}^2 = \frac{3}{2}\frac{U}{C} - \frac{1}{2} + \left[1 + 3\left(\frac{U}{C}\right)^2\right]^{1/2}, \quad (3.21)$$

and this relation is plotted in Fig. 1 as the dashed curve. Notice once again that the radius of the critical circle contracts to zero if $U + C = 0$. In this case all wavenumbers are unstable. In contrast to the slab ($\mu = \infty$), ML in section 2, the geostrophic ($\mu = 0$) ML is unstable for all values of U/C. And in both cases all wavenumbers are unstable if $U + C = 0$.

One qualitative difference between the cases $\mu = \infty$ and $\mu = 0$ is the behavior of the instability at high wavenumbers. In the geostrophic case ($\mu = 0$) the growth rate increases linearly with k if $\mathcal{L}^2p^2 \to \infty$. From (3.19) and (3.20), one has

$$\omega_i \approx \frac{|C|}{\sqrt{3}}k, \quad (3.22)$$

if $\mathcal{L}^2p^2 \gg 1$. In the slab case ($\mu = \infty$) the shortest waves grow the fastest, but at least the growth rate is bounded as $\mathcal{L}^2p^2 \to \infty$ [e.g., see (2.22)]. The ultraviolet divergence in (3.22) is discussed below in section 4.

To make an a posterori assessment of the validity of the SML approximation, we must check that ω/f is small. To take an extreme case, suppose that $C = 0.1$ m s^{-1} and $k = 1$ km^{-1}. Then from (3.22) it follows that $\omega/f = 1/\sqrt{3}$, which is not convincingly small. For frontal disturbances with frequencies comparable to f the SML approximation is not valid, and in the present case this means that the dispersion relation is inaccurate as $k \to \infty$.

Some of the results in this section are anticipated by the work of Fukamachi et al. (1995). In their section 4 they discuss the stability of a vertically sheared ML starting from the momentum equations rather than the SML approximation. Attention is confined to the case $U + C = 0$ so that FMP find the instability at all wavenumbers, which occurs when the base of the ML is flat. FMP emphasized that there were only minor differences between the dispersion relation of the slab case [e.g., (2.18)] and that of the vertically sheared case [e.g., (3.17)]. Indeed, this is true if $U + C = 0$, but in general there are differences between the two dispersion relations. The most significant consequence of these differences is that in the slab case the instability occurs only when $UC < 0$, while in the geostrophic case the instability is present no matter the sign of UC. In both cases if $U + C \neq 0$, then the base of the ML slopes and low wavenumbers are stabilized.

e. Linearized thermohaline gradient alignment

In the linear problem in (1.8) the basic state has parallel temperature and salinity gradients. Small initial perturbations will then introduce some nonalignment of the thermohaline gradients. The evolution of these perturbations can be understood by projecting the initial disturbance onto the three modes (F, S, and BC) and evolving the eigenmodes according to the linear dynamics described above. This solution is accurate until the disturbance reaches nonlinear amplitude.

The linearized dynamics of thermohaline gradient alignment are contained in the results (3.9) and (3.12). The F and S modes make no contribution to $\mathcal{J}$ in (3.9) because their eigenvectors have $\tilde{\sigma}/\tilde{\theta} = \Gamma_\sigma/\Gamma_\theta$: in other words, the nonaligned structure in the initial perturbation does not project onto the F and S modes. Thus, the unstable exponential growth of these two modes neither creates nor amplifies nonaligned structure in the thermohaline fields.

The BC mode carries all of the thermohaline Jacobian $\mathcal{J}$, and according to either (3.12) or (3.16) this mode decays exponentially. [The BC decay rate in (3.16) vanishes if $k = 0$ but in this case it follows from (3.9) that $\mathcal{J} = 0$ anyway.] Thus, nonaligned initial perturbations decay as $t \to \infty$ even though there are unstable linear modes.

4. Curing the ultraviolet divergence: Stable stratification and dissipation

The divergence of the growth rate in (3.22) as $k \to \infty$ raises the question of a high wavenumber cutoff for

the instability. In this section we will compare two different mechanisms that prevent the blowup in (3.22):

(i) The addition of scale selective dissipation such as diffusion $\kappa\nabla^2\xi$ and viscosity $\nu\nabla^4\psi$ to the SML model.

(ii) The effects of stable vertical stratification in the ML.

The viscosity and diffusion in (i) might represent unresolved smaller-scale processes in the ML; for example, Langmuir circulations or diurnal convection could produce horizontal mixing on scales of 100 m. With respect to point (ii), the SML approximation does predict that the ML is vertically statified [see (4.2) and (4.3) below], but this stable vertical stratification does not appear at leading order in the expansion scheme. The evolution equations in (1.4)–(1.7) take no account of the higher-order stable stratification. This is an important difference between the SML approximation and earlier studies of baroclinic instability such as Eady (1949) and Stone (1966, 1970): in these earlier works the vertical buoyancy gradient is imposed externally and its strength is independent of the horizontal buoyancy gradients. By contrast, in the SML approximation, the vertical buoyancy gradients are dynamically related to the horizontal buoyancy gradients as in (4.2) below, or $N^2 = M^4/f^2$ in the notation of Tandon and Garrett (1994).

a. The Eady problem and stable stratification

We begin consideration of point (ii) by recalling the main features of the classic Eady problem for baroclinic instability. The Eady problem and the SML approximation are similar in that one considers a vertically sheared, rapidly rotating flow such as (3.2). In the Eady problem stable stratification, with a buoyancy frequency conventionally denoted by N^2, is included in the basic state. But in the SML approximation the stable stratification of the ML is a higher-order effect. Thus, no parameter corresponding to N^2 appears in the analysis of section 3. This is the essential difference between the Eady problem and the SML instability. [An inessential difference is that in the Eady problem the bottom is rigid, while in the SML case the bottom of the layer is free to deform. This difference is irrelevant for high wavenumbers.]

The Eady dispersion relation is shown in Fig. 10 by the solid curve [e.g., see Gill 1982, Eq. (13.3.5); Pedlosky 1987, Eq. (7.7.18)]. There is a high wavenumber cutoff at

$$k_E = 2.4\frac{f}{N\mathcal{H}}. \tag{4.1}$$

It is remarkable that the cutoff at k_E is independent of the magnitude of the thermal wind. The dashed line, which is tangent to the Eady growth rate at $k = 0$, is

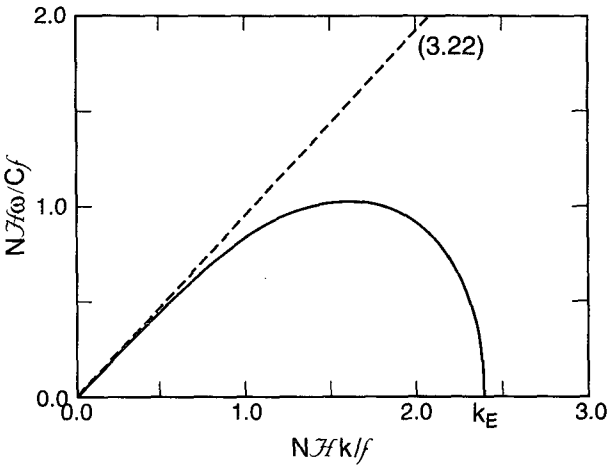

FIG. 10. The growth rate of the Eady wave as a function of wavenumber k with $l = 0$. The dashed straight line is the SML result in (3.22).

the SML result in (3.22). From this comparison we learn that stable stratification in the mixed layer, though often ignored, has an important role in stabilizing high wavenumbers against baroclinic instability. Physically, this is because short waves produce relatively upright fluid displacements that lie outside of Eady's "wedge of instability." The more nearly horizontal particle trajectories in long waves lie within the wedge of instability and so can release potential energy.

The comparison in Fig. 10 also shows that the instability described in section 3 is a special case ($N = 0$) of the well-known quasigeostrophic baroclinic instability. The same cannot be said of the superficially similar instability described in section 2. In the slab limit the velocity within the ML is independent of depth, and the slanting particle trajectories described by Eady are not possible. This is a further illustration of the qualitative difference between the slab and geostrophic MLs.

We can now use recent results on mixed layer restratification to make a rough estimate of k_E in (4.1): we must estimate N within the ML. The SML approximation makes a prediction concerning N^2 in the ML. In the notation of this paper the expansion of the density is

$$\rho = \check{\rho}\left\{1 - \frac{f}{g\mathcal{H}}\left[\xi + \tau\mu(1+\mu^2)^{-1}\nabla\xi\cdot\nabla\xi \times\left(\frac{z}{\mathcal{H}} + \frac{1}{2}\right) + \cdots\right]\right\}, \tag{4.2}$$

where the ellipses indicate higher-order terms in the SML expansion. Using the linearized result $\nabla\xi\cdot\nabla\xi \approx 4C^2$, one can now estimate from (4.2) that

$$N^2 \equiv -\frac{g\rho_z}{\check{\rho}} \approx (1+\mu^2)^{-1}\frac{\tau}{\tau_U}\frac{4C^2}{\mathcal{H}^2}, \qquad (4.3)$$

where we have used $\mu = 1/f\tau_U$. Putting (4.3) into the expression for k_E in (4.1) gives

$$k_E^{-1} \approx (1+\mu^2)^{-1/2}\left(\frac{\tau}{\tau_U}\right)^{1/2}\frac{2C}{f}. \qquad (4.4)$$

Now if (i) heat salt and momentum all mix at the same rate so that $\tau/\tau_U \sim 1$ and (ii) the ML is geostrophic so $\mu \ll 1$ and (iii) the buoyancy gradient is typical of frontal regions so that $C \sim 10$ cm s^{-1} and $f \sim 10^{-4}$ s^{-1}, then from (4.37)

$$k_E^{-1} \sim 2 \text{ km}. \qquad (4.5)$$

Notice that with $\mathcal{H} \sim 100$ m, the estimates above give $N/f \sim 20$ in the ML.

Tandon and Garrett (1994) have recently produced a model of mixed layer restratification after a sudden mixing event. In their notation $N^2 = M^4/f^2$, where $M = -f\Gamma_\zeta/\mathcal{H}$ is the horizontal buoyancy gradient. This result of Tandon and Garrett is the same as (4.3) provided that $\tau/\tau_U = 1$ and $\mu \ll 1$.

b. *Scale selective dissipation*

We turn now to the possibility of high wavenumber stabilization by scale selective dissipation. In the usual ad hoc fashion we add a terms $\kappa\nabla^2\sigma'$ and $\kappa\nabla^2\theta'$ to the right-hand side of (3.10a,b) and $\nu\mathcal{L}^2\nabla^4\psi'$ to the right-hand side of (3.10c). With this addition the generalization of the dispersion relation (3.17) is

$$(\Omega + i\kappa p^2)(\Omega\mathcal{L}^2p^2 + \omega + i\nu\mathcal{L}^2p^4) + C\left(\frac{1}{3}C\mathcal{L}^2p^2k - \omega\right)k = 0. \qquad (4.6)$$

The high wavenumber behavior of this dispersion relation is isolated by the approximation

$$(\Omega + i\kappa p^2)(\Omega\mathcal{L}^2p^2 + i\nu\mathcal{L}^2p^4) + \frac{1}{3}C^2\mathcal{L}^2p^2k^2 \approx 0. \qquad (4.7)$$

The terms dropped in passing from (4.6) to (4.7) correspond to deformation of the base of the ML. In making the approximation (4.7) we have also assumed that the viscosity ν and diffusion κ are small in a sense that is quantified below in the discussion after (4.9).

The solution of (4.7) is

$$\omega_\pm = Uk + i\left[-\frac{1}{2}(\kappa+\nu)p^2 \pm \sqrt{\frac{1}{3}C^2k^2 + \frac{1}{4}(\kappa-\nu)^2p^4}\right]. \qquad (4.8)$$

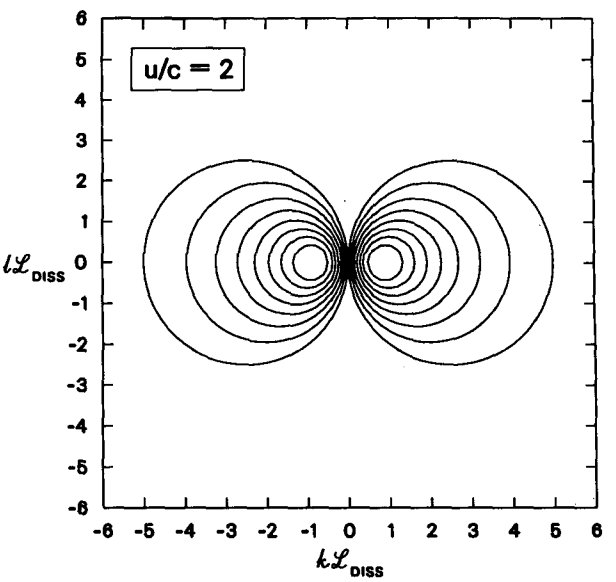

FIG. 11. Curves of constant growth rate in the wavenumber plane calculated from (4.32) with $U/C = 2$ and $\nu/C\mathcal{L}_{DISS} = \kappa/C\mathcal{L}_{DISS} = 0.1$. The growth rate is zero on the two outermost circles.

The circular contours of constant growth rate in the (k, l) plane are shown in Fig. 11. The neutral stability condition $\omega_{+i} = 0$ shows that the dissipation produces a high wavenumber cutoff so that waves shorter than the dissipation length

$$\mathcal{L}_{DISS} \equiv \frac{\sqrt{3\nu\kappa}}{|C|} \qquad (4.9)$$

are stable. The one slightly surprising fact to emerge from this analysis is that both viscosity and diffusion are required to give a high wavenumber cutoff. For the high wavenumber approximation in (4.7) to be valid, the dissipation must be weak, so that $\mathcal{L} \gg \mathcal{L}_{DISS}$.

Suppose that the diffusion and viscosity are produced by some process that overturns the ML isotropically so that the horizontal mixing distance scales with the depth $\mathcal{H} \sim 100$ m of the ML. As a nominal value of the mixing time we take $\tau \sim 10^5$ s, so that the overturning velocities are of order $\mathcal{H}/\tau \sim 10^{-3}$ m s^{-1}. Then $\nu \sim \kappa \sim \mathcal{H}^2/\tau \sim 0.1$ m^2 s^{-1}. We previously estimated $C \sim 0.005$ m s^{-1} for climatological temperature gradients. With these numbers the dissipation length is

$$\mathcal{L}_{DISS} \sim 3 \text{ m}. \qquad (4.10)$$

Even if our estimates of ν and κ were small by a factor of 100 (as they might be for strong Langmuir circulations), the instability would extend down to lengths at which the dynamics is certainly not geostrophic. [Note that in frontal regions C can be a factor of 20 larger than the value of 1/2 cm s^{-1} used in the estimate (4.10).] Comparing (4.5) with (4.10) we see that $k_E^{-1} \gg \mathcal{L}_{DISS}$, so that it is most likely stable stratification,

rather than scale selective dissipation, that imposes a high wavenumber cutoff on ML baroclinic instability.

5. Discussion and conclusions

In this paper we have used the subinertial mixed layer approximation to discuss the low-frequency disturbances that can exist in a ML and exploit the peculiar stratification found in this region. We have made a comparison of two limiting model assumptions. First there is the slab ML, in which case the horizontal velocity has no vertical shear because of rapid mixing of vertical momentum. The complementary limit is the geostrophic ML, in which case the horizontal velocity is sheared according to the thermal wind relation.

The differences between the two cases are qualitative. For instance, in the geostrophic case thermohaline gradient alignment can act to tighten the $T-S$ relation. This process, relying as it does on shear dispersion, is absent in the slab limit. In the geostrophic case the SML approximation reproduces the low-wavenumber behavior of the Eady baroclinic instability problem. Although there is an instability in the slab case, the relation to the Eady problem is obscure: the slab velocity profile means that the usual physical interpretation of baroclinic instability in terms of slanting particle displacements releasing potential energy is inapplicable.

In the geostrophic ML, which we believe is more realistic, disturbances with inverse wavenumbers between about 2 km and 10 km are unstable. These numbers, 2 km and 10 km, should not be taken too literally because the actual values depend sensitively on details of the basic state, particularly the inclination of the ML base (e.g., see Fig. 1) and the buoyancy frequency within the ML. The low wavenumber cutoff (i.e., waves with inverse wavenumber longer than about 10 km are stable) is associated with the deformation of the ML base: the relevant length scale is $\mathcal{L} \equiv \sqrt{g'\mathcal{H}}/f$, where $\mathcal{H}$ is ML depth. The high wavenumber cutoff (i.e., waves with inverse wavenumber shorter than 2 km are stable) is associated with the weak vertical stratification within the ML: the relevant length scale is $k_E^{-1} \sim N\mathcal{H}/f$, where N is the buoyancy frequency within the ML. The essential point is that the peculiar stratification of the ML[1] ensures that $\mathcal{L} \gg k_E^{-1}$, and so there is generally a band of unstable waves. The length scales suggested by this calculation are rather shorter than those usually associated with the mesoscale eddy field, and this finding supports the hypothesis that small-scale fronts in the ML are the result of shallow baroclinic instability.

[1] A weakly stratified layer with $N/f \leq 20$ bounded below by an almost discontinuous increase in density so that $g' \sim 10^{-2}$ m s^{-2}.

Acknowledgments. WRY is supported by the National Science Foundation (OCE93-01462) and the CHAMMP program (DOE DEFG03 93ER61690). Lianggui Chen is the recipient of a UCAR ocean modeling fellowship. We thank John Marshall, Jay McCreary, and Joe Pedlosky for useful comments on this paper and Lisa Lehman for her assistance with the computations.

REFERENCES

Batchelor, G. K., 1959: Small-scale variation of convected quantities like temperature in a turbulent fluid. *J. Fluid Mech.*, **5**, 113–139.

de Szoeke, R. A., 1980: On the effects of horizontal variability of wind stress on the dynamics of the ocean mixed layer. *J. Phys. Oceanogr.*, **10**, 1439–1454.

——, and J. G. Richman, 1984: On wind-driven mixed layers with strong horizontal gradients—a theory with applications to coastal upwelling. *J. Phys. Oceanogr.*, **14**, 364–377.

Eady, E., 1949: Long waves and cyclone waves. *Tellus*, **1**, 33–52.

Fukamachi, Y., J. P. McCreary, and J. A. Proehl, 1995: Instability of density fronts in layer and continuously stratified models. *J. Geophys. Res.*, in press.

Gill, A. E., 1982: *Atmosphere–Ocean Dynamics.* Academic Press, 662+ xv pp.

Halliwell, G. R., and Coauthors, 1991: Descriptive oceanography during the frontal air–sea interaction experiment: Medium- to large-scale variability. *J. Geophys. Res.*, **96**, 8553–8567.

McCreary, J. P., and P. K. Kundu, 1988: A numerical investigation of the Somali current during the southwest monsoon. *J. Mar. Res.*, **46**, 1–23.

——, and Z. Yu, 1992: Equatorial dynamics in a $2\frac{1}{2}$-layer model. *Progress in Oceanography*, Vol. 29, Pergamon Press, 61–132.

Niiler, P. P., and R. W. Reynolds, 1984: The three-dimensional circulation near the eastern North Pacific subtropical front. *J. Phys. Oceanogr.*, **14**, 217–230.

Pedlosky, J. P., 1987: *Geophysical Fluid Dynamics.* Springer-Verlag, 710+ xiv pp.

Rhines, P. B., 1976: The dynamics of unsteady currents. *The Sea*, Vol. 6, E. D. Goldberg, Ed., Wiley and Sons, 189–318.

Ripa, P., 1993: Conservation laws for primitive equation models with inhomogeneous layers. *Geophys. Astrophys. Fluid Dyn.*, **70**, 85–111.

Salmon, R., 1980: Baroclinic instability and geostrophic turbulence. *Geophys. Astrophys. Fluid Dyn.*, **15**, 167–211.

Samelson, R. M., and C. A. Paulson, 1988: Towed thermistor chain observations of fronts in the subtropical North Pacific. *J. Geophys. Res.*, **93**, 2237–2246.

Schopf, P. S., and M. A. Cane, 1983: On equatorial dynamics, mixed layer physics and sea surface temperature. *J. Phys. Oceanogr.*, **13**, 917–935.

Stone, P. H., 1966: On non-geostrophic baroclinic stability. *J. Atmos. Sci.*, **23**, 390–400.

——, 1970: On non-geostrophic baroclinic stability. Part II. *J. Atmos. Sci.*, **27**, 721–726.

Tandon, A., and C. J. R. Garrett, 1994: A note on mixed layer restratification due to a horizontal density gradient. *J. Phys. Oceanogr.*, **24**, 1419–1424.

Taylor, G. I., 1953: Dispersion of soluble matter in solvent flowing slowly down a tube. *Proc. Roy. Soc. London Ser. A.*, **219**, 186–203.

Young, W. R., 1994: The subinertial mixed layer approximation. *J. Phys. Oceanogr.*, **24**, 1812–1826.